Available online at www.sciencedirect.com
ScienceDirect
Journal of Computational Physics 221 (2007) 330–348
JOURNAL OF COMPUTATIONAL PHYSICS
www.elsevier.com/locate/jcp

Calculation of the vacuum Green's function valid even for high toroidal mode numbers in tokamaks

M.S. Chance [a,*], A.D. Turnbull [b], P.B. Snyder [b]

[a] *Plasma Physics Laboratory, Theory Department, P.O. Box 451, Princeton University, Princeton, NJ 08543, USA*
[b] *General Atomics, San Diego, CA 92186-5068, USA*

Received 23 February 2006; accepted 8 June 2006
Available online 17 August 2006

Abstract

The present evaluation of the Green's function used for the magnetic scalar potential in vacuum calculations for axisymmetric geometry has been found to be deficient even for moderately high, n, the toroidal mode number. This is relevant to the edge localized peeling-ballooning modes calculated by GATO, PEST and other MHD stability codes. The deficiency was due to the loss of numerical precision arising from the upward recursion relation used for generating the functions from the values at $n = 0$ from the complete elliptic integrals of the first and second kinds. To ameliorate this, a direct integration of the integral representation of the function is crafted to achieve the necessary high accuracy for moderately high mode numbers, with due consideration to the singular behavior of the integrand involved. At higher mode numbers the loss of numerical precision due to cancellations from the oscillatory behavior of the integrand is further avoided by judiciously deforming the integration contour into the complex plane to obtain a new integral representation for the Green's function. Near machine precision, roughly 12–16 digits, can be achieved by using a combination of these techniques. The relation to the associated Legendre functions, as well as a novel integral representation of these are also described.

MSC: 65D15; 65D30

PACS: 52.65.Cc; 52.55.Fa

Keywords: Tokamak vacuum Green's function; Legendre function; Integral representation; Recursion relation

1. Introduction

The magnetic scalar potential that is needed to include the effects of the vacuum region in stability calculations in axisymmetric toroidal configurations requires an accurate evaluation of the free space Green's function, $\mathscr{G}$, in two dimensions. Historically the emphasis in fusion research has been on the external kink modes with low order toroidal mode numbers, n. The present evaluation that is used to calculate the Green's function

* Corresponding author. Tel.: +1 609 243 2058.
E-mail addresses: chance@pppl.gov (M.S. Chance), turnbull@fusion.gat.com (A.D. Turnbull), snyder@fusion.gat.com (P.B. Snyder).

0021-9991/$ - see front matter
doi:10.1016/j.jcp.2006.06.025

in the GATO, ERATO [1–3] and PEST [4,5] codes relies on an upward recursion relation in the toroidal mode number, n, initiated from the complete elliptic functions of the first and second kinds, K and E, respectively. However, significant loss of digits occurs when these codes are used for studying even moderately high n MHD modes. (Note that the pseudo-vacuum version of ERATO avoids the calculation of the Green's function and the associated singularities altogether. It, however, has a different set of numerical problems, for example, it cannot be used for very distant walls or a wall at infinity.) This problem has recently become more critical because of the emerging importance of the moderately high n (typically $3 < n < 30$) peeling/ballooning modes in tokamaks which are being studied, for example, by the ELITE code [6,7]. At present the elliptic integrals are only confidently calculated at most to roughly eight digits using relations from [8]. A few recursions in n can quickly lead to a complete loss of accuracy. While the evaluations of the elliptic integrals have been replaced with the much more accurate recursive method of Bulirsch [9,10], this only postponed the problem to a few more increments in n. These observations motivated the present work to devise other methods to evaluate the Green's function accurately in the range where the present methods fail.

In addition to n, it is found that the numerical properties of the Green's function also depend on the other characterization of the integrand, namely the parameter $\hat{\rho} \equiv [\{(X-X')^2 + (Z-Z')^2\}/4XX']^{1/2}$, the normalized distance between source and observer points in the X–Z plane, where the notation is such that the radius vector $\boldsymbol{r} = (X, \phi, Z)$ in cylindrical coordinates. It is evident that $\hat{\rho}$ can take on a wide range of values – small values, for example, when the source and observer points are situated on the same surface; and large values when the normalizing denominator gets small in small aspect ratio configurations and/or when the distance between the source and observer is large in configurations that are vertically elongated or contain distant vacuum vessels, for example. When $\hat{\rho}$ vanishes, the integrand has an integrable singularity which gives rise to the logarithmic behavior of the Green's function. The numerical difficulties associated with this singular behavior are addressed in the numerical algorithms. It is found that the salient properties of the function that are relevant to this work are, to a large extent, dependent on the product $n\hat{\rho}$.

As an alternative to using the recursion relation for $n\hat{\rho} \gtrsim 1$ an algorithm is constructed which directly integrates an integral representation of $\mathscr{G}$ for arbitrary $n\hat{\rho}$. To avoid the difficulties associated with the singular behavior of the integrand we extract the singular behavior and use a suitable change of variable to efficiently perform the quadratures. Maintaining the periodicity of the integrand enables us to take advantage of the extremely high accuracy offered by the trapezoidal rule because of the Euler–MacLaurin effect [11]. This is found to be very accurate, attaining machine precision for $n\hat{\rho} \ll 1$. However, as $n\hat{\rho}$ increases the method begins to suffer from the limitation of the machine precision because the oscillatory behavior of the integrand results in roundoff errors, limiting the range of $n\hat{\rho}$, for example, to $\lesssim 10$ for six digit accuracy in $\mathscr{G}$. This is avoided by crafting another method of integration which suitably deforms the integration contour into the infinite complex ϕ plane so that the integrand, rather than oscillating, decays exponentially and is positive definite. In this case Gaussian quadratures are used for the integration on a suitable finite range. As checks, the integrands in both these cases are expanded in finite power series and integrated analytically. In practice, all the methods of integration can be used with the desired accuracy apropos to the value of $\hat{\rho}$. To illustrate the points made, sets of results for suitable values of $\hat{\rho}$ and n are presented, each containing the numerical data from the methods described – the recursion method, the trapezoidal integration, the Gaussian quadrature along the new contour of integration and their analytic series integrations. The attributes and deficiencies of each method are then easily compared. In order to give this work a wider perspective the relation to the associated Legendre functions is provided.

The paper is structured as follows. Section 2 describes the two dimensional Green's function and the techniques used to deal with the its singular behavior when $n\hat{\rho} \ll 1$. To facilitate the discussion of the limitation of the recursion method that motivated this work, the more accurate trapezoidal technique is described in Section 3 since the actual numerical results from both can later be compared. The roundoff problem associated with the trapezoidal techniques when $n\hat{\rho} \sim 1$ is discussed here as well. In Section 4 the recursion relation method used for evaluating the function for moderately high values of n is described together with its breakdown when n and ρ are large. Section 5 deals with the integration of the analytical series expansion of the integrand in $\hat{\rho}^{-2}$. Section 6 describes the new integral representation which is valid for all ranges of n and $\hat{\rho}$ and in particular is accurate for large values of n and ρ, thus complementing the methods of the previous sections. The results of expanding the new integrand in a suitable power series valid for finite $\hat{\rho}$ are also presented here. The summary and conclusions are presented finally in Section 7, where we also suggest a prescription for obtaining the Green's

function to at least 12 digits over a much wider range of $n\hat{\rho}$ than previously achieved. The relationship between the Green's function algorithm and the associated Legendre functions is presented in Appendix A, where it is also shown that a novel integral representation of these functions results from this relationship.

2. The two dimensional Green's function

In this section the treatment of the singular behavior of the Green's function in the two dimensional space (X, Z) is described. This entails regularizing the integrand by subtracting its zeroth order singular contribution to facilitate treating the resulting integral with a suitably accurate quadrature scheme. The subtracted piece is in turn accurately calculated and then added back to complete the solution. A judicious change of variable also proved helpful. It turns out that this technique is very effective when $\hat{\rho} \ll 1$, but the onset of roundoff errors renders the results unacceptable when $n\hat{\rho} \gtrsim 10$. These observations will be clarified and quantified when actual numerical results are shown for relevant ranges of $\hat{\rho}$ and n.

2.1. Treatment of the singularity

Integration of the free space Green's function in cylindrical coordinates over the toroidal angle ϕ', gives the two dimensional Green's function in (X, Z):

$$\mathscr{G}^n \equiv \frac{1}{2\pi} \oint \frac{e^{in(\phi-\phi')}}{|\mathbf{r}-\mathbf{r}'|} d\phi' \tag{1}$$

and since

$$|\mathbf{r}-\mathbf{r}'|^2 = X^2 + X'^2 + (Z-Z')^2 - 2XX'\cos(\phi-\phi') \tag{2}$$

this can be written as

$$\mathscr{G}^n = \frac{1}{2\pi} \oint d\phi \frac{e^{-in\phi}}{\sqrt{\rho^2 + 4XX'\sin^2(\phi/2)}}, \tag{3}$$

$$= \frac{1}{2\pi\sqrt{XX'}} \int_{-\pi/2}^{\pi/2} d\phi \frac{\cos 2n\phi}{\sqrt{\hat{\rho}^2 + \sin^2\phi}}, \tag{4}$$

where $\hat{\rho}^2 = \rho^2/4XX'$, with $\rho^2 = (X-X')^2 + (Z-Z')^2$. Examination of Eq. (4) shows that the singular behavior of $\mathscr{G}^n$ occurs when $\hat{\rho} \to 0$ since the denominator vanishes when $\phi \to 0$. This gives rise to the logarithmic dependence in the integral as can be seen if the leading singular term is extracted by writing $\mathscr{G}^n$ as

$$2\pi\sqrt{XX'}\mathscr{G}^n = \int_{-\pi/2}^{\pi/2} d\phi' \frac{\cos 2n\phi' - \cos\phi'}{\sqrt{\hat{\rho}^2 + \sin^2\phi'}} + \int_{-\pi/2}^{\pi/2} d\phi' \frac{\cos\phi'}{\sqrt{\hat{\rho}^2 + \sin^2\phi'}}, \tag{5}$$

$$\equiv 2\pi\sqrt{XX'}[\mathscr{G}_{\text{reg}} + \mathscr{G}_{\text{sing}}]. \tag{6}$$

The regularized integrand of $\mathscr{G}_{\text{reg}}$ is now non-infinite as $\rho \to 0$, and the leading singularity contained in $\mathscr{G}_{\text{sing}}$ can be evaluated analytically,

$$2\pi\sqrt{XX'}\mathscr{G}_{\text{sing}} = 2\left[-\log\hat{\rho} + \log(1+\sqrt{\hat{\rho}^2+1})\right]. \tag{7}$$

Thus,

$$\mathscr{G}^n \underset{\hat{\rho}\to 0}{\to} -\frac{1}{\pi\sqrt{XX'}}\log\hat{\rho}. \tag{8}$$

The integral of Eq. (4) can be integrated directly while paying due attention to the singular properties of the integrand. If the integrand is periodic over its range of integration, the trapezoidal rule offers remarkable accuracy because of the Euler–MacLaurin effect [11]. As written, the integrand of Eq. (4) is periodic in ϕ and the

pathology that occurs for small values of $\hat{\rho}$ could be handled by subtracting the singular behavior as above in Eq. (5). However, the subtracted portion there is unfortunately not periodic. So instead, we replace the $\cos\phi$ term in Eq. (5) with unity, that is:

$$2\pi\sqrt{XX'}\mathscr{G}^n = \int_{-\pi/2}^{\pi/2} \mathrm{d}\phi' \frac{\cos 2n\phi' - 1}{\sqrt{\hat{\rho}^2 + \sin^2\phi'}} + \int_{-\pi/2}^{\pi/2} \mathrm{d}\phi' \frac{1}{\sqrt{\hat{\rho}^2 + \sin^2\phi'}} \tag{9}$$

and $\mathscr{G}_{\text{sing}}$ in this case is,

$$2\pi\sqrt{XX'}\mathscr{G}_{\text{sing}} = \int_{-\pi/2}^{\pi/2} \mathrm{d}\phi' \frac{1}{\sqrt{\hat{\rho}^2 + \sin^2\phi'}}, \tag{10}$$

$$= \frac{2}{\sqrt{\hat{\rho}^2 + 1}} K(k), \tag{11}$$

where $K(k)$ can be accurately calculated using previously established methods, e.g. that of Bulirsch [9,10]. A plot of the integrand with and without the subtraction is shown in Figs. 1 and 2 for $\hat{\rho} = 0.01$ and $n = 10$. As can be seen, even though the integrand is mathematically well conditioned, the behavior at $\phi \sim 0$ is still not comfortably smooth enough for efficient numerical analysis. We therefore introduce a change of variable that effectively packs the grid in the neighborhood of the singularity,

$$\phi' = \phi - \delta \sin 2\phi, \tag{12}$$

$$\text{with} \quad \mathrm{d}\phi' = (1 - 2\delta\cos 2\phi)\mathrm{d}\phi. \tag{13}$$

The choice of $\delta = 0.5$ is optimal since $\mathrm{d}\phi' \underset{\phi\to 0}{\to} 2\phi^2\,\mathrm{d}\phi$, which corresponds to maximal grid packing. The transformed integrands in both instances are shown in Figs. 3 and 4. Without the regularization of Eq. (9) this transformation introduces new local extrema at $\phi_m \sim \pm 1.285\hat{\rho}^{1/3}$ where the integrand takes on the value $\sim 1.906\hat{\rho}^{-1/3}$, both leading only to mildly singular behavior. In practice, if $\hat{\rho}$ is not extremely small, it is often sufficient to just use the transformation given in Eq. (12) without the regularization since it accomplishes both goals of packing the grid points and almost regularizing the integrand at the singular point. Using both the regularization and transformation with $\delta = 0.5$ could be a bit of overkill. It's significant to note that the change of variable in Eq. (13) preserves the periodicity of the integrand which is crucial for satisfying the Euler–MacLaurin requirement.

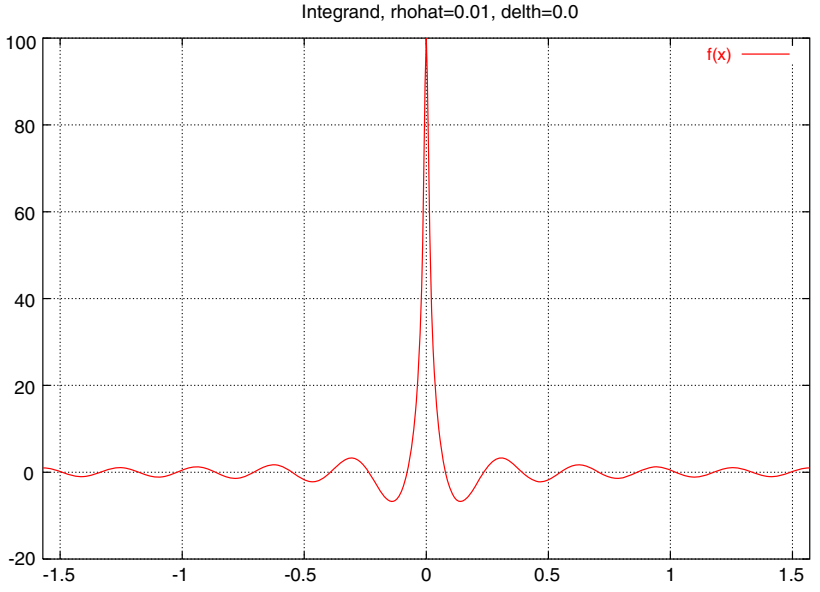

Fig. 1. The integrand of $\mathscr{G}^n$ in Eq. (4) with $\hat{\rho} = 0.01$ and $n = 10$.

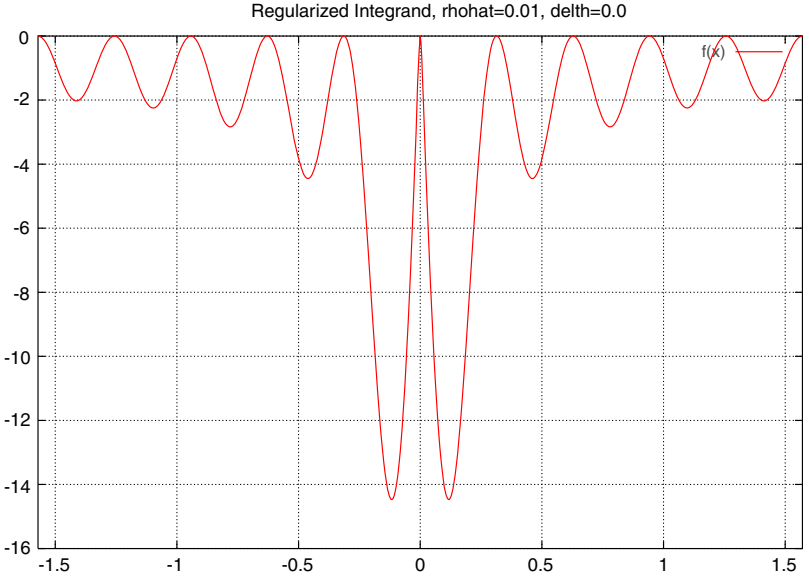

Fig. 2. The regularized integrand of Eq. (5) with $\hat{\rho} = 0.01$ and $n = 10$.

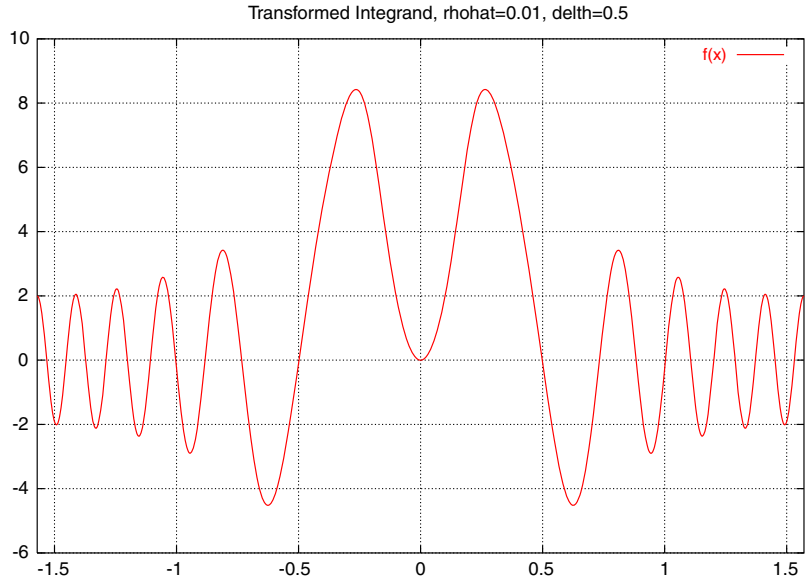

Fig. 3. The integrand of $\mathscr{G}^n$ showing the effect of the change of variable $\phi' = \phi - \delta \sin 2\phi$.

3. The trapezoidal integration algorithm

3.1. Results when $n\hat{\rho} \ll 1$

A demonstration of how well the numerical implementation of these techniques work when $\hat{\rho}$ is small is shown in the tables where the result from the trapezoidal integration is carried out for various values of the parameters $\hat{\rho}$ and n, using an increasing number of grid points, m, starting from 16 and doubled several times to check the convergence of the algorithm. In the tables, the result from the integration is denoted by $\mathscr{G}_m$ and the quantity $d\mathscr{G}_m/\mathscr{G}_m$ is the relative difference between the present and previous m points integration,

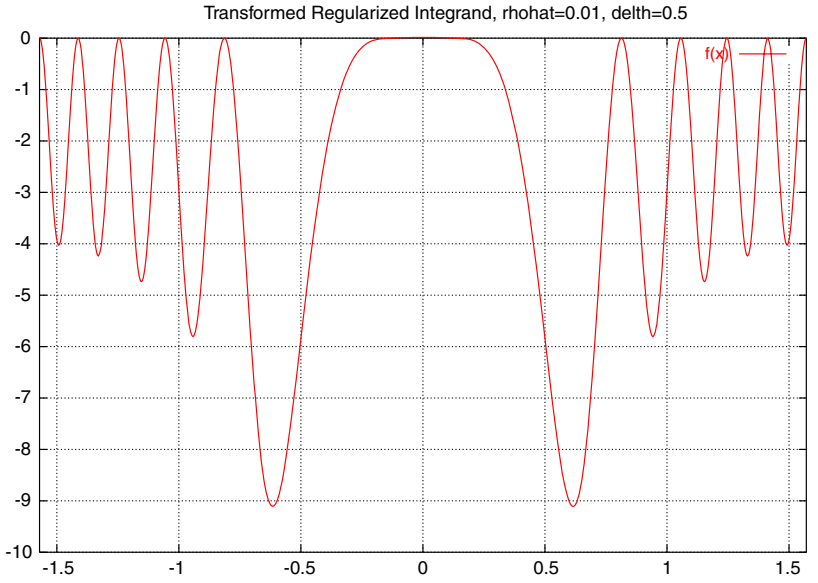

Fig. 4. The regularized integrand of $\mathscr{G}^n$ showing the effect of the change of variable $\phi' = \phi - \delta \sin 2\phi$.

$(\mathscr{G} - \mathscr{G}_{\text{prev}})/\mathscr{G}_{\text{prev}}$. The label '$K$ for regularization' in the header indicates whether or not the integrand is regularized using Eq. (9) and the method used to evaluate K in $\mathscr{G}_{\text{sing}}$. In all cases δ is set at 0.5.

The results in Table 1 for $n = 1$ and 21 with $\hat{\rho} = 10^{-3}$ indicate that without the regularization, roughly 128 points will produce a relative error of $\sim 10^{-7}$ and 512 points achieves near machine precision of 14–16 digits accuracy. The results for the same cases but with the regularization is shown in Table 2. The same accuracies can be achieved with 16 points for $n = 1$, 64 points for $n = 21$, and 256 points for near machine precision.

It should be noted here that since any breakdown of the accuracy of the trapezoidal technique can be easily ascertained from the value of $d\mathscr{G}_m/\mathscr{G}_m$ in the tables, the results of this technique are useful to gauge the accuracy of other methods used for calculating $\mathscr{G}^n$ as long as the values of $\hat{\rho}$ and n are within the regime where the trapezoidal method is accurate, the latter of course depending on the accuracy of the K used if the integral is regularized according to Eq. (9).

In the tables the relative errors between some of the various pairs of methods are denoted by ε. The relative difference $d\mathscr{G}_m/\mathscr{G}_m$ and the relative error ε can take on large values if one (or both) of the pair that is being compared is wildly inaccurate if, e.g. it is evaluated for parameters that are outside the range of validity of the method.

3.2. Results when $\hat{\rho} \gtrsim 1$

When $\hat{\rho} \gtrsim 1$ the integrand is well behaved but tends toward a constant amplitude as illustrated in Fig. 5; for large n the oscillatory behavior of the integrand causes a Riemann–Lebesgue-like cancellation of the positive and negative contributions so that the resulting integral can be extremely small. The subtractions required for this lead to loss of digits in the numerical implementation as it stands. An illustration of this is in Table 3 (upper) where the results for $\hat{\rho} = 0.7$ and $n = 21$ are shown. As indicated by the lack of decrease of the relative error, $d\mathscr{G}_m/\mathscr{G}_m$, as m is increased, an accuracy of roughly four digits is achievable. Complete breakdown of the method is seen when $n = 26$ in Table 3 (lower). Clearly then, for these moderately high values of n and $\hat{\rho}$, an alternative algorithm is necessary for applications in this range. This issue will be addressed below in Section 6.

4. The recursion relation

As shown in Appendix A, $\mathscr{G}^n$ can be written in terms of the associated Legendre functions $P^n_{-1/2}$ and this allows us to make use of their properties in our applications. For example, the recursion relation for $P^n_{-1/2}$ has

Table 1
Results of the integration without regularization

n	$\hat{\rho}$	K for regularization			K, E for recursion	
1	1.0E−03	None			Bulirsch	
Method		$\mathscr{G}$	$\varepsilon_{\text{trap}}$	$\varepsilon_{\text{expan}}$	ε_{eul}	$\varepsilon_{\text{gauss}}$
Trapezoidal	m	$\mathscr{G}_m$	$d\mathscr{G}_m/\mathscr{G}_m$			
	16	1.800624975390113E+00				
	32	2.025355996644204E+00	1.11E−01			
	64	2.003834472493246E+00	−1.07E−02			
	128	2.003460279443467E+00	−1.87E−04			
	256	2.003460125056524E+00	−7.71E−08			
	512	2.003460125056492E+00	−1.60E−14			
	1024	2.003460125056489E+00	−1.55E−15			
Recursion		2.003460125056489E+00	0.00E+00			
High-n exp.		−1.200893356599288E+20	−5.99E+19			
High-n Eul exp.		−4.666191255321733E+17	−2.33E+17			
Gauss, $n_g = 64$		2.003460148769300E+00	1.18E−08	−1.00E+00	−1.00E+00	
Large $\hat{\rho}$, $l = 10$		1.296496874848175E+67	6.47E+66			6.47E+66

n	$\hat{\rho}$	K for regularization			K, E for recursion	
21	1.0E−03	None			Bulirsch	
Method		$\mathscr{G}$	$\varepsilon_{\text{trap}}$	$\varepsilon_{\text{expan}}$	ε_{eul}	$\varepsilon_{\text{gauss}}$
Trapezoidal	m	$\mathscr{G}_m$	$d\mathscr{G}_m/\mathscr{G}_m$			
	16	9.707300403760134E−01				
	32	8.469965739481430E−01	−1.46E−01			
	64	1.046917853500563E+00	1.91E−01			
	128	1.046543371969088E+00	−3.58E−04			
	256	1.046543217454265E+00	−1.48E−07			
	512	1.046543217454232E+00	−3.18E−14			
	1024	1.046543217454229E+00	−2.76E−15			
Recursion		1.046543217454264E+00	3.39E−14			
High-n exp.		−1.379714064081404E+10	−1.32E+10			
High-n Eul exp.		−4.824432908770844E+07	−4.61E+07			
Gauss, $n_g = 64$		1.046543217454232E+00	3.33E−15	−1.00E+00	−1.00E+00	
Large $\hat{\rho}$, $l = 10$		1.176489578342860E+180	1.12E+180			1.12E+180

been used to generate the Green's function for $n > 1$ and the corresponding recursion relation for $\mathscr{G}^n$, as derived in Appendix A is,

$$\mathscr{G}^{n+1} = \frac{4n(2\hat{\rho}^2+1)}{(2n+1)}\mathscr{G}^n - \frac{2n-1}{2n+1}\mathscr{G}^{n-1}, \tag{14}$$

for $n = 1, 2, \ldots$ In the GATO code an equivalent recursion is done directly on its version of the integral representation, Eq. (4) [2]. In both cases, as shown in Appendix A, the recursion is initiated at $n = 1$ from the relations of $P^0_{-1/2}$ and $P^0_{1/2}$ to the complete elliptic integrals of the first and second kinds, K and E, respectively.

$$\mathscr{G}^0 = \frac{1}{\pi\sqrt{XX'}}\frac{K(k)}{\sqrt{\hat{\rho}^2+1}}, \tag{15}$$

$$\mathscr{G}^1 = \frac{1}{\pi\sqrt{XX'}}\frac{(2\hat{\rho}^2+1)K(k) - 2(\hat{\rho}^2+1)E(k)}{\sqrt{\hat{\rho}^2+1}}, \tag{16}$$

$$\text{with} \quad k^2 \equiv \frac{1}{\hat{\rho}^2+1}. \tag{17}$$

The accuracy of the calculation of $\mathscr{G}^n$ is thus dependent on the stability of the recursion relation and the numerical precision of the elliptic integrals. In the VACUUM [5] and GATO [1,2] codes the polynomial approximations from Abramowitz and Stegun [8] are used which are accurate to $O(10^{-8})$. Since $\mathscr{G}^n$ is positive, in

Table 2
Results of the integration with the regularization applied

n	$\hat{\rho}$	K for regularization			K, E for recursion	
1	1.0E−03	Bulirsch			Bulirsch	
Method		$\mathscr{G}$	$\varepsilon_{\text{trap}}$	$\varepsilon_{\text{expan}}$	ε_{eul}	$\varepsilon_{\text{gauss}}$
Trapezoidal	m	$\mathscr{G}_m$	$d\mathscr{G}_m/\mathscr{G}_m$			
	16	2.003460269450408E+00				
	32	2.003460149376894E+00	−5.99E−08			
	64	2.003460125712500E+00	−1.18E−08			
	128	2.003460125056781E+00	−3.27E−10			
	256	2.003460125056490E+00	−1.45E−13			
	512	2.003460125056490E+00	0.00E+00			
	1024	2.003460125056489E+00	−4.43E−16			
Recursion		2.003460125056489E+00	0.00E+00			
High-n exp.		−1.200893356599288E+20	−5.99E+19			
High-n Eul exp.		−4.666191255321733E+17	−2.33E+17			
Gauss, $n_g = 64$		2.003460148769300E+00	1.18E−08	−1.00E+00	−1.00E+00	
Large $\hat{\rho}$, $l = 10$		1.296496874848175E+67	6.47E+66			6.47E+66

n	$\hat{\rho}$	K for regularization			K, E for recursion	
21	1.0E−03	Bulirsch			Bulirsch	
Method		$\mathscr{G}$	$\varepsilon_{\text{trap}}$	$\varepsilon_{\text{expan}}$	ε_{eul}	$\varepsilon_{\text{gauss}}$
Trapezoidal	m	$\mathscr{G}_m$	$d\mathscr{G}_m/\mathscr{G}_m$			
	16	1.173565334436309E+00				
	32	8.251007266808328E−01	−4.22E−01			
	64	1.046543506719816E+00	2.12E−01			
	128	1.046543217582401E+00	−2.76E−07			
	256	1.046543217454231E+00	−1.22E−10			
	512	1.046543217454231E+00	4.24E−16			
	1024	1.046543217454232E+00	2.12E−16			
Recursion		1.046543217454264E+00	3.12E−14			
High-n exp.		−1.379714064081404E+10	−1.32E+10			
High-n Eul exp.		−4.824432908770844E+07	−4.61E+07			
Gauss, $n_g = 64$		1.046543217454232E+00	6.66E−16	−1.00E+00	−1.00E+00	
Large $\hat{\rho}$, $l = 10$		1.176489578342860E+180	1.12E+180			1.12E+180

Eq. (14) a subtraction takes place at each upward increment in n as the recursion progresses. This causes a loss of accuracy which worsens as $\hat{\rho}$ increases. For example, after j recursions the two leading terms in the expansion very roughly scale like $[2(2\hat{\rho}^2+1)]^j$ times $E(\hat{\rho})$ and $K(\hat{\rho})$. For $\hat{\rho} = 0.7$ (e.g. an NSTX or MAST case $\hat{\rho}_{\max} \sim a/R \sim 0.7$, where a/R signifies the inverse aspect ratio), 10^8 precision (the precision of the standard expansions for E and K) is lost for $n \sim 9$, and 10^{15} precision is lost for $n = 15$. This is illustrated in Table 4 (upper). The result of using the recursion method and its relative error, $\varepsilon_{\text{trap}}$, compared with the trapezoidal method is in the row denoted by 'recursion', and within this method, the entry '*A&S*' under the header 'K, E for recursion' denotes that the polynomial expressions from [8] is used for the elliptical integrals in the recursion method. For moderate values of $\hat{\rho}(\sim 0.5)$ an accuracy of only four digits is obtained at $n = 5$. For $\hat{\rho} \sim 1$ the same accuracy is obtained at only $n = 3$, Table 4 (lower). At $n = 5$ only the first significant digit is accurately calculated (not shown). Evidently the accuracy of this method is clearly dependent on the precision with which the K and E are calculated. We have substituted the much more precise algorithms of [9,10], indicated by 'Bulirsch' in Table 5, which achieve near machine precision, but as seen this only delays the onset of the problem: for $\hat{\rho} = 0.5$ only three digits accuracy is obtainable at $n = 15$. For $\hat{\rho} \sim 1$ complete loss of accuracy occurs at $n = 13$. Clearly then, as was found for the Riemann–Lebesgue-like cancellation problem with the trapezoidal method, for these moderately high values of n and $\hat{\rho}$, alternative algorithms must be devised to evaluate $\mathscr{G}^n$ in this regime.

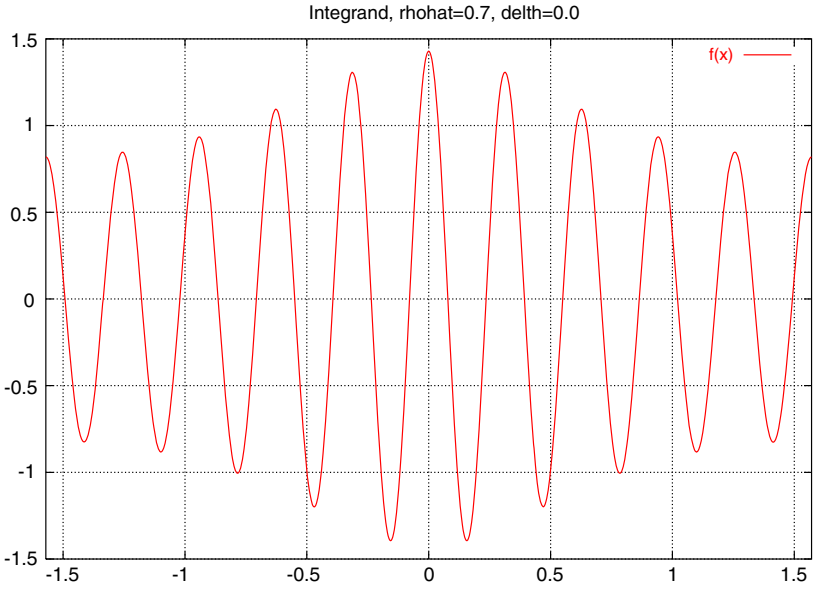

Fig. 5. The almost constant amplitude of the integrand of $\mathscr{G}^n$ when $\hat{\rho} = 0.7$.

We remark here that we have tried the algorithm for K by Carlson [12,13] but found it not as accurate as Bulirsch's at very small values of $\hat{\rho}$. On the other hand the algorithm in [8] is much more accurate there than its advertised accuracy of $\sim 10^{-8}$.

5. Series expansion in $\hat{\rho}^{-2}$

For $\hat{\rho} > 1$ the square root in Eq. (4) can be expanded in a convergent series in $\sin^2\phi/\hat{\rho}^2$, so that,

$$\mathscr{G}^n = \frac{1}{2\pi\sqrt{XX'}} \int_{-\pi/2}^{\pi/2} \mathrm{d}\phi \frac{\cos 2n\phi}{\hat{\rho}} \sum_{l=0}^{\infty} \binom{-1/2}{l} \frac{\sin^{2l}\phi}{\hat{\rho}^{2l}}, \tag{18}$$

$$= \frac{1}{2\sqrt{XX'}} \frac{1}{\hat{\rho}} \sum_{l=n}^{\infty} \frac{(-1)^n}{(2\hat{\rho})^{2l}} \binom{2l}{l-n} \binom{-1/2}{l}, \tag{19}$$

or

$$\mathscr{G}^n = \frac{1}{\sqrt{XX'}} \frac{(-1)^n}{(2\hat{\rho})^{2n+1}} \sum_{l=0}^{\infty} \frac{1}{(2\hat{\rho})^{2l}} \binom{2(l+n)}{l} \binom{-1/2}{l+n}, \tag{20}$$

where

$$\binom{p}{q} = \frac{p(p-1)\cdots(p-q+1)}{1\cdot 2\cdots q}, \qquad \binom{p}{0} = 1, \tag{21}$$

$$= \frac{p!}{q!(p-q)!}, \tag{22}$$

and the expression used here for the integral over ϕ can be found in [14]. The numerical implementation of this serves as another check against other methods for calculating $\mathscr{G}^n$. The results are denoted in the tables with the row labeled 'large $\hat{\rho}$.' $l+1$ is the number of term used in the series, Eq. (20). $\varepsilon_{\mathrm{trap}}$, $\varepsilon_{\mathrm{gauss}}$ denote the relative error of the results compared with those of the trapezoidal and the Gaussian methods, the latter of which is to be described in Section 6. As can be seen from the results for $n = 3$, $\hat{\rho} = 3.0$ in Table 6, the series converges fairly rapidly. For these values of n and $\hat{\rho}$, all the methods are quite accurate but the region of validity for the present expansion does not overlap those of the previously presented methods sufficiently enough to effectively complement them. This will be discussed in Section 7.

Table 3
Results showing the Riemann–Lebesgue like cancellations in the trapezoidal rule

n	$\hat{\rho}$	K for regularization			K, E for recursion	
21	7.000E−01	None			Bulirsch	
Method		$\mathcal{G}$	$\varepsilon_{\text{trap}}$	$\varepsilon_{\text{expan}}$	ε_{eul}	$\varepsilon_{\text{gauss}}$
Trapezoidal	m	$\mathcal{G}_m$	$d\mathcal{G}_m/\mathcal{G}_m$			
	16	−6.274082791960794E−02				
	32	−1.447698537538380E−01	5.67E−01			
	64	−5.968361308644754E−11	−2.43E+09			
	128	8.249520858094606E−14	7.24E+02			
	256	8.264894844900450E−14	1.86E−03			
	512	8.241259237540266E−14	−2.87E−03			
	1024	8.239665460346712E−14	−1.93E−04			
Recursion		1.851608323673001E−06	2.25E+07			
High-n exp.		8.233536091075646E−14	−7.44E−04			
High-n Eul exp.		8.233536091673747E−14	−7.44E−04			
Gauss, $n_g = 64$		8.233536091210725E−14	−7.44E−04	1.64E−11	−5.62E−11	
Large $\hat{\rho}$, $l = 10$		5.282645234352444E+00	6.42E+13			6.42E+13

n	$\hat{\rho}$	K for regularization			K, E for recursion	
26	7.000E−01	None			Bulirsch	
Method		$\mathcal{G}$	$\varepsilon_{\text{trap}}$	$\varepsilon_{\text{expan}}$	ε_{eul}	$\varepsilon_{\text{gauss}}$
Trapezoidal	m	$\mathcal{G}_m$	$d\mathcal{G}_m/\mathcal{G}_m$			
	16	8.537481649732798E−02				
	32	−8.489516044564373E−02	2.01E+00			
	64	2.968671991045776E−05	2.86E+03			
	128	−4.423544863740858E−16	6.71E+10			
	256	−3.070460552478949E−16	−4.41E−01			
	512	−2.732189474663471E−17	−1.02E+01			
	1024	−4.803015624110785E−17	4.31E−01			
Recursion		1.135228162431733E−03	−2.36E+13			
High-n exp.		1.084634837534896E−16	−3.26E+00			
High-n Eul exp.		1.084634837552541E−16	−3.26E+00			
Gauss, $n_g = 64$		1.084634837538194E−16	−3.26E+00	3.04E−12	−1.32E−11	
Large $\hat{\rho}$, $l = 10$		8.688359715604025E−01	−1.81E+16			8.01E+15

6. An alternative representation for $\mathcal{G}^n$

As found above, for moderately large values of $n\hat{\rho} \sim 1$, the recursion methods fail and, in the trapezoidal method, the oscillatory behavior of the integrand with almost constant amplitude causes a cancellation of the positive and negative contributions which results in an unacceptable loss of digits. To prevent this we examine the properties of the integrand in complex ϕ plane and deform the contour of integration appropriately to avoid the oscillatory behavior of the integrand. In terms of the now complex $\phi \equiv u + \mathrm{i}v$ the integrand in Eq. (4) becomes

$$\mathcal{G}^n = \frac{2}{\pi\sqrt{XX'}}\mathcal{R}e\int_{-\pi/2}^{\pi/2}\frac{\mathrm{e}^{2\mathrm{i}n\phi}\mathrm{d}\phi}{\sqrt{\hat{\rho}^2+\sin^2\phi}}, \tag{23}$$

$$= \frac{2}{\pi\sqrt{XX'}}\mathcal{R}e\int_{-\pi/2}^{\pi/2}\frac{\mathrm{e}^{2\mathrm{i}n(u+\mathrm{i}v)}\mathrm{d}\phi}{\sqrt{\hat{\rho}^2+(\sin u\cosh v-\mathrm{i}\cos u\sinh v)^2}}. \tag{24}$$

Within the range of interest, $-\pi/2 < u < \pi/2$, the relevant branch points occur at $u = 0$, $v = \pm v_0$ where

Table 4
Results of the recursion method initiated from the elliptic integrals from the expressions in [8]

n	$\hat{\rho}$	K for regularization			K, E for recursion	
5	5.000E−01	None			*A&S*	
Method		$\mathscr{G}$	$\varepsilon_{\text{trap}}$	$\varepsilon_{\text{expan}}$	ε_{eul}	$\varepsilon_{\text{gauss}}$
Trapezoidal	m	$\mathscr{G}_m$	$d\mathscr{G}_m/\mathscr{G}_m$			
	16	1.142611060415834E−03				
	32	1.328805434947195E−03	1.40E−01			
	64	1.328805434681813E−03	−2.00E−10			
	128	1.328805434681833E−03	1.48E−14			
	256	1.328805434681812E−03	−1.60E−14			
	512	1.328805434681821E−03	7.18E−15			
	1024	1.328805434681817E−03	−2.94E−15			
Recursion		1.328673947058222E−03	−9.90E−05			
High-n exp.		1.328789444382180E−03	−1.20E−05			
High-n Eul exp.		1.328807456406867E−03	1.52E−06			
Gauss, $n_g = 64$		1.328805434681792E−03	−1.88E−14	1.20E−05	−1.52E−06	
Large $\hat{\rho}$, $l = 10$		3.504857328980133E+06	2.64E+09			2.64E+09

n	$\hat{\rho}$	K for regularization			K, E for recursion	
3	1.00	None			*A&S*	
Method		$\mathscr{G}$	$\varepsilon_{\text{trap}}$	$\varepsilon_{\text{expan}}$	ε_{eul}	$\varepsilon_{\text{gauss}}$
Trapezoidal	m	$\mathscr{G}_m$	$d\mathscr{G}_m/\mathscr{G}_m$			
	16	6.623739047580020E−04				
	32	6.623536627594768E−04	−3.06E−05			
	64	6.623536627594941E−04	2.60E−14			
	128	6.623536627594724E−04	−3.27E−14			
	256	6.623536627594654E−04	−1.05E−14			
	512	6.623536627594542E−04	−1.70E−14			
	1024	6.623536627595157E−04	9.30E−14			
Recursion		6.623151919219140E−04	−5.81E−05			
High-n exp.		6.623498857663590E−04	−5.70E−06			
High-n Eul exp.		6.623542696708142E−04	9.16E−07			
Gauss, $n_g = 64$		6.623536627594345E−04	−1.23E−13	5.70E−06	−9.16E−07	
Large $\hat{\rho}$, $l = 10$		3.690808208088648E−03	4.57E+00			4.57E+00

$$v_0 = \sinh^{-1}\hat{\rho}. \tag{25}$$

The corresponding branch cuts are chosen as shown in Fig. 6. Also shown is the deformed contour of integration which is chosen to be in the upper half plane to ensure that the integrand vanishes when $v \to \infty$. The contributions along the segments $u = \pm\pi/2$, $0 \leqslant v \leqslant \infty$ cancel each other (a consequence of our choice of the integration range from $-\pi/2$ to $\pi/2$), and there is no contribution from the branch point, so we are left with equal contributions from both sides of the branch cut along the positive imaginary axis,

$$\mathscr{G}^n = \frac{4}{\pi\sqrt{XX'}}\mathscr{R}e\int_{v_0}^{\infty}\frac{ie^{-2nv}\,dv}{\sqrt{\hat{\rho}^2 - \sinh^2 v}}. \tag{26}$$

Setting $v \equiv v_0 + z/2n$ this becomes

$$\mathscr{G}^n = \frac{2e^{-2nv_0}}{n\pi\sqrt{XX'}}\int_0^{\infty}\frac{e^{-z}\,dz}{\sqrt{\sinh^2(v_0 + z/2n) - \hat{\rho}^2}}, \tag{27}$$

$$= \frac{2e^{-2nv_0}}{n\pi\sqrt{XX'}}\int_0^{\infty}\frac{e^{-z}dz}{\sqrt{(2\hat{\rho}^2+1)\sinh^2(z/2n) + \hat{\rho}(\hat{\rho}^2+1)^{1/2}\sinh(z/n)}}, \tag{28}$$

Table 5
Results of the recursion method initiated from the elliptic integral calculated by the Bulirsch algorithms [10]

n	$\hat{\rho}$	K for regularization			K, E for recursion	
15	5.000E−01	None			Bulirsch	
Method		$\mathcal{G}$	$\varepsilon_{\text{trap}}$	$\varepsilon_{\text{expan}}$	ε_{eul}	$\varepsilon_{\text{gauss}}$
Trapezoidal	m	$\mathcal{G}_m$	$d\mathcal{G}_m/\mathcal{G}_m$			
	16	−2.406135953645585E−01				
	32	−5.721420479838883E−02	−3.21E+00			
	64	5.178946813413909E−08	1.10E+06			
	128	5.178946823442779E−08	1.94E−09			
	256	5.178946844291987E−08	4.03E−09			
	512	5.178946786829272E−08	−1.11E−08			
	1024	5.178946782969512E−08	−7.45E−10			
Recursion		5.182477372450577E−08	6.82E−04			
High-n exp.		5.178946767960794E−08	−2.90E−09			
High-n Eul exp.		5.178946802075638E−08	3.69E−09			
Gauss, $n_g = 64$		5.178946781067901E−08	−3.67E−10	2.53E−09	−4.06E−09	
Large $\hat{\rho}$, $l = 10$		9.876966032775818E+08	1.91E+16			1.91E+16

n	$\hat{\rho}$	K for regularization			K, E for recursion	
13	1.00	None			Bulirsch	
Method		$\mathcal{G}$	$\varepsilon_{\text{trap}}$	$\varepsilon_{\text{expan}}$	ε_{eul}	$\varepsilon_{\text{gauss}}$
Trapezoidal	m	$\mathcal{G}_m$	$d\mathcal{G}_m/\mathcal{G}_m$			
	16	−4.713699776418764E−04				
	32	−1.667230403506501E−03	7.17E−01			
	64	7.270259047564843E−12	2.29E+08			
	128	7.270388067623368E−12	1.77E−05			
	256	7.270441193529820E−12	7.31E−06			
	512	7.270888318505753E−12	6.15E−05			
	1024	7.270899919468998E−12	1.60E−06			
Recursion		−9.694701998690181E−08	−1.33E+04			
High-n exp.		7.270904580650855E−12	6.41E−07			
High-n Eul exp.		7.270904582429580E−12	6.41E−07			
Gauss, $n_g = 64$		7.270904581130163E−12	6.41E−07	6.59E−11	−1.79E−10	
Large $\hat{\rho}$, $l = 10$		1.966969889744283E−06	2.71E+05			2.71E+05

Table 6
Results for $n = 3$, $\hat{\rho} = 3.0$. For these values, all methods shown are fairly accurate

n	$\hat{\rho}$	K for regularization			K, E for recursion	
3	3.0	None			Bulirsch	
Method		$\mathcal{G}$	$\varepsilon_{\text{trap}}$	$\varepsilon_{\text{expan}}$	ε_{eul}	$\varepsilon_{\text{gauss}}$
Trapezoidal	m	$\mathcal{G}_m$	$d\mathcal{G}_m/\mathcal{G}_m$			
	16	9.240693979034598E−07				
	32	9.263881421339369E−07	2.50E−03			
	64	9.263881421235284E−07	−1.12E−11			
	128	9.263881421187579E−07	−5.15E−12			
	256	9.263881421155054E−07	−3.51E−12			
	512	9.263881421160474E−07	5.85E−13			
	1024	9.263881421078617E−07	−8.84E−12			
Recursion		9.263874878011383E−07	−7.06E−07			
High-n exp.		9.263882053755038E−07	6.83E−08			
High-n Eul exp.		9.263877502044503E−07	−4.23E−07			
Gauss, $n_g = 64$		9.263881420990642E−07	−9.50E−12	−6.83E−08	−4.23E−07	
Large $\hat{\rho}$, $l = 10$		9.263881421776629E−07	7.53E−11			8.48E−11

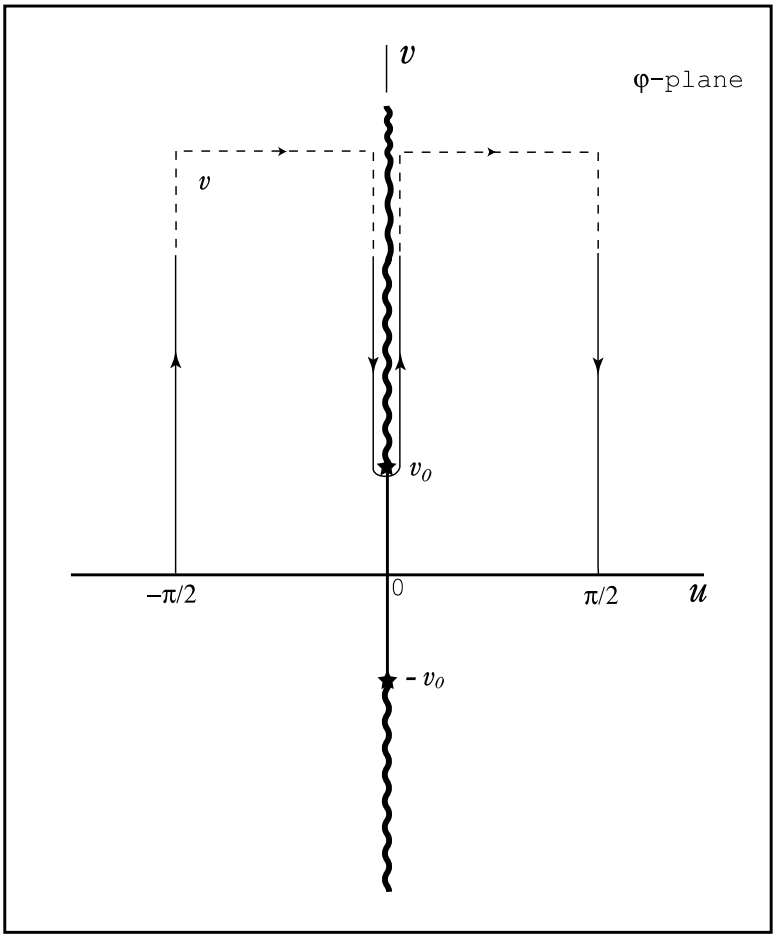

Fig. 6. The complex $\phi = u + iv$ plane showing the branch points at $v_0 = \pm\sinh^{-1}\hat{\rho}$, the corresponding branch cuts denoted by the wavy lines, and the new deformed contour of integration which was originally along the real axis over the range $[-\pi/2, +\pi/2]$.

where we used Eq. (25). The integrand is now non-oscillatory and positive definite leaving the residual of the cancellations, alluded to previously when $n\hat{\rho}$ is large, in the exponential factor, e^{-2nv_0}.

The expression in the square root in the denominator of Eq. (27) can be expanded in a power series in z about $z = 0$. With $\zeta \equiv z/2n$,

$$\sinh^2(v_0+\zeta) - \hat{\rho}^2 = (2\hat{\rho}^2+1)\sinh^2\zeta + \hat{\rho}(\hat{\rho}^2+1)^{1/2}\sinh(2\zeta) \tag{29}$$

$$= A\zeta\left[1 + B\zeta + C\zeta^2 + \frac{B}{3}\zeta^3 + D\zeta^4\right. \tag{30}$$

$$+ \frac{2B}{45}\zeta^5 + E\zeta^6 + \frac{B}{315}\zeta^7 + F\zeta^8 \tag{31}$$

$$\left. + \frac{2B}{14175}\zeta^9 + G\zeta^{10} + \cdots\right], \tag{32}$$

where

$$A \equiv 2\hat{\rho}\sqrt{\hat{\rho}^2+1}, \qquad B \equiv \frac{2\hat{\rho}^2+1}{2\hat{\rho}\sqrt{\hat{\rho}^2+1)}}, \tag{33}$$

$$C \equiv \frac{2}{3}, \qquad D \equiv \frac{2}{15}, \qquad E \equiv \frac{4}{315}, \tag{34}$$

$$F \equiv \frac{2}{2835}, \qquad G \equiv \frac{4}{155925}, \tag{35}$$

using $\cosh v_0 = \sqrt{\hat{\rho}^2 + 1}$. Further analysis gives,

$$\frac{1}{\sqrt{\sinh^2(v_0+\zeta) - \hat{\rho}^2}} \approx \left(\frac{2n}{A}\right)^{1/2} \frac{1}{z^{1/2}} \sum_{l=1}^{8} \alpha_l z^{l-1}, \tag{36}$$

where

$$\alpha_1 = 1.0, \qquad \alpha_2 = -\frac{B}{4n}, \qquad \alpha_3 = \frac{1}{4n^2}\left(\frac{3}{8}B^2 - \frac{1}{3}\right), \tag{37}$$

$$\alpha_4 = -\frac{B}{16n^3}\left(\frac{5}{8}B^2 - \frac{2}{3}\right), \qquad \alpha_5 = \frac{1}{16n^4}\left(\frac{35}{128}B^4 - \frac{3}{8}B^2 + \frac{1}{10}\right), \tag{38}$$

$$\alpha_6 = -\frac{B}{368640n^5}(2835B^4 - 4800B^2 + 1984), \tag{39}$$

$$\alpha_7 = \frac{1}{61931520n^6}(218295B^6 - 441000B^4 + 254016B^2 - 31232), \tag{40}$$

$$\alpha_8 = -\frac{B}{49545216n^7}(81081B^6 - 190512B^4 + 141120B^2 - 31744). \tag{41}$$

When substituted into Eq. (27) each term in the series can be expressed in terms of the gamma function, Γ,

$$\mathscr{G}^n \approx \frac{2[\hat{\rho}^2 + \sqrt{\hat{\rho}^2+1}]^{-2n}}{\pi\sqrt{XX'}} \left(\frac{2}{nA}\right)^{1/2} \sum_{l=1}^{8} \alpha_l \Gamma\left(\frac{2l-1}{2}\right), \tag{42}$$

where we used

$$e^{v_0} = \hat{\rho}^2 + \sqrt{\hat{\rho}^2 + 1} \tag{43}$$

and the gamma functions are evaluated from $\Gamma(p+1) = p\Gamma(p)$ with $\Gamma(1/2) = \sqrt{\pi}$.

One can also numerically evaluate the integral Eq. (28) directly, but it's first convenient to introduce yet another change of variable, $z = t^2$, so that

$$\mathscr{G}^n = \frac{4\sqrt{2}e^{-2nv_0}}{n\pi\sqrt{XX'A}} \int_0^\infty \frac{te^{-t^2}\,dt}{\sqrt{2B\sinh^2(t^2/2n) + \sinh(t^2/n)}}, \tag{44}$$

where the constants A and B are defined in Eq. (33). For $\hat{\rho} \neq 0$ the integrand is well behaved and is amenable to an appropriate quadrature scheme like for example Gaussian quadratures. Because of the strong Gaussian decay of the integrand, sufficient accuracy can still be obtained in practical applications if the range of integration is finite. If $\hat{\rho} \ll 1$, one could devise methods to deal appropriately with the integration, but the recursion method, for example, is already suitably accurate in that regime.

Numerical results from the eight-term expansion, Eq. (42) and the integration of Eq. (44) where a 64 point Gaussian integration is used in the range $t = [0, 7]$, are given in all of the tables. The row labeled 'high-n exp.', and $\varepsilon_{\text{trap}}$, is the result from the eight-term expansion, and its relative error compared with result from the trapezoidal rule. The row labeled 'high-n Eul exp.' indicates the results from using Wijngaarden implementation of the Euler transformation to attempt to accelerate the convergence of the series [9] and $\varepsilon_{\text{trap}}$ is the relative error compared with the trapezoidal method. The row labeled 'Gauss' is the result from the integration of Eq. (44); n_g is the order of the quadrature used. The relative errors compared with the results from the trapezoidal rule, $\varepsilon_{\text{trap}}$, and the series expansion Eq. (42), $\varepsilon_{\text{expan}}$, are shown for this method. Evidently this integral representation is valid over a wide range of ρ and n whereas as expected the expansion is valid only for the subspace where $n\hat{\rho}$ is at least moderately large. The strong Gaussian decay of the integrand enabled the infinite range of integration to be curtailed to only $t = [0, 7]$. These points will be more elucidated in the next section.

7. Summary and conclusions

We have presented a variety of methods to calculate the two dimensional Green's function that is needed in Green's second identity to evaluate the magnetic scalar potential in the vacuum region in tokamak geometry

[1,5]. This was motivated by the shortcomings uncovered when the original algorithms failed when benchmarking the GATO MHD [2] code with the moderately high toroidal mode number, n, calculations of the ELITE code [6,7]. The highly numerically efficient algorithms that were used previously in GATO and PEST depended on an upward recursion relation in n that was initiated from the elliptic integrals of the first and second kinds. These were calculated using polynomials approximations found in [8] that were accurate to $O(10^{-8})$. The much more accurate iterative algorithms of [9,10] postponed the unacceptable loss of digits due to the recursion relation to a moderately higher value of n but the recursion still ultimately failed. These observations depend strongly on the value of $\hat{\rho}$, the normalized distance between the source and observer points in the two dimensional, $(X–Z)$, space, with the unacceptable breakdown of the recursion method occurring when $\hat{\rho} \sim 1$ for $n \sim 5$–10.

One alternative method to calculate $\mathscr{G}^n$ to complement the accurate evaluations offered by the recursion methods at small $n\hat{\rho}$ was to integrate the Green's function equation (4) directly using appropriate techniques to deal with the singular behavior of the kernel, and maintaining its periodicity to take advantage of the unique accuracy offered by using the trapezoidal rule for the quadratures. This enabled us to attain near machine accuracy ($\sim 12-16$ digits) when $n\hat{\rho} \lesssim 10$. Beyond these ranges of $\hat{\rho}$ and n the algorithm begins to be compromised in accuracy because the integrand in Eq. (4) becomes highly oscillatory and tends to almost constant amplitude. The almost equal contributions of the positive and negative contributions of the integrand again result in an unacceptable loss of digits. To avoid this, the oscillatory behavior of the integrand is suppressed by deforming the contour of integration into the complex ϕ plane so that the integrand instead decays exponentially and the resultant of the aforementioned cancellations is explicitly factored from the (now positive definite) integrand of Eq. (44). This is reminiscent of a combination of the well known constant phase and saddle point methods in the evaluation of integrals. Evaluation of the ensuing integral over a suitable finite range $[0,5]$ using a 32 point Gaussian quadrature is more than sufficient to provide near machine precision accuracy for any practical value of n over a large range of $n\hat{\rho}$. A more precise 64 point quadrature over $[0,7]$ was also incorporated. At large $n\hat{\rho}$ an analytical evaluation of the integrand to an eight-term series expansion of the integral provides an accurate check and an even more numerically efficient scheme for obtaining $\mathscr{G}^n$. This can of course be generalized to include more terms in the series, thereby increasing the range of applicability as needed.

There is a great deal of overlap in the parameter space of $\hat{\rho}$–n where the various methods of evaluating $\mathscr{G}^n$ may be acceptably accurate. In practice, the recursion method can be used for low $n\hat{\rho}$ applications as is done at present – or perhaps a low order trapezoidal direct quadrature. For moderately high values of $n\hat{\rho}$ the trapezoidal method would suffice. For very high values of these parameters the Gaussian method or the series expansion can be applied. A graphical depiction of the accuracy properties is shown in the figures. In Fig. 7 are plotted lines of constant relative error, $\varepsilon = 10^{-6}$, in the n vs. $\hat{\rho}$ plane for various algorithms – trapezoidal (dotted line), the recursion (short dashed line), the eight-term series expansion of Eq. (42) (solid line), and the large $\hat{\rho}$ expansion of Eq. (20) with $l = 10$, (long dashed line). The arrow attached to each curve indicates the direction where the relative error decreases from 10^{-6}. The dot-dashed line at upper right denotes where the value of the integral approximately approaches the underflow limit, $\sim 10^{-300}$. The recursion method with the more accurate elliptical integral gives an accuracy of at least 10^{-6} over most of the region when $n\hat{\rho} \lesssim 6$. The trapezoidal integration method offers the same accuracy for $n\hat{\rho} \lesssim 10$. On the other hand, analytically expanding and integrating Eq. (27) give the same accuracy when $n\hat{\rho} \gtrsim 4$.

The much more accurate Gaussian integration of the new integral representation of Section 6 is shown in the n vs. $\hat{\rho}$ plane of Fig. 8 over eight orders of magnitude in $\hat{\rho}$. The three straight lines on the left show the results of using a Gaussian integration of Eq. (44). Dashed line: $\varepsilon = 10^{-6}$ with 64 points over the range $[0,7]$. Solid line: $\varepsilon = 10^{-9}$ using 64 points in $[0,7]$, and this also closely represents $\varepsilon = 10^{-6}$ for 32 points in $[0,5]$. Dotted line: $\varepsilon = 10^{-9}$ using 32 points in $[0,5]$. In the same figure, the two lines on the right correspond to $\varepsilon = 10^{-9}$ for the trapezoidal (dotted line) and recursion (dashed line) methods. The arrows indicate the direction where the relative error decreases. The 64 point quadrature over the range $[0,7]$ ensures an accuracy of better than 10^{-9} for $n\hat{\rho} \gtrsim 2 \times 10^{-3}$, and better than 10^{-6} for $n\hat{\rho} \gtrsim 3 \times 10^{-4}$. The accuracy of the 32 point Gaussian quadrature over the range $[0,5]$ is better than 10^{-6} for $n\hat{\rho} \gtrsim 2 \times 10^{-3}$, and better than 10^{-9} for $n\hat{\rho} \gtrsim 1.5 \times 10^{-2}$ over a range $[0,5]$. The accuracy of the Gaussian integration can be extended over a wider domain if appropriate steps are taken to deal with the behavior of the integrand when $\hat{\rho} \ll 1$.

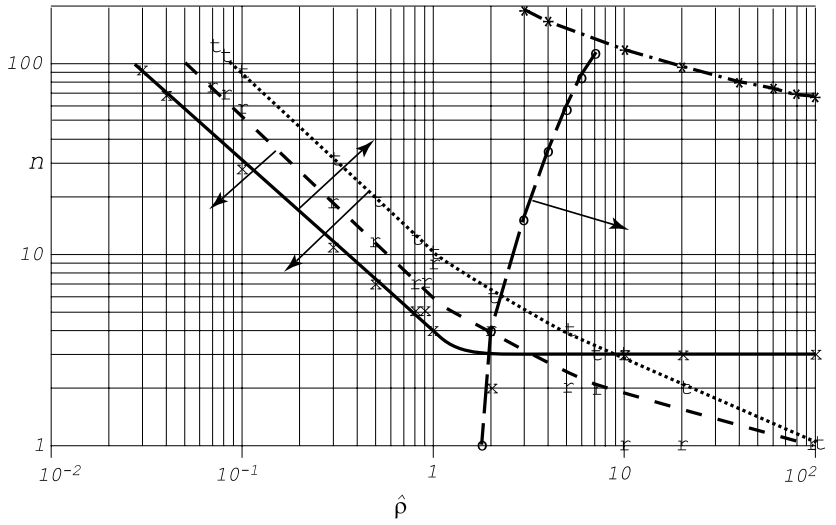

Fig. 7. Lines of constant relative error, ε, in the n vs. $\hat{\rho}$ plane for various algorithms – trapezoidal (dotted line), the recursion (short dashed line), the series expansion (solid line), and the large $\hat{\rho}$ expansion (long dashed line). The arrows indicate the direction where the relative error decreases from 10^{-6}. The dot-dashed line at upper right denotes where the value of the integral approximately approaches the underflow limit, $\sim 10^{-300}$.

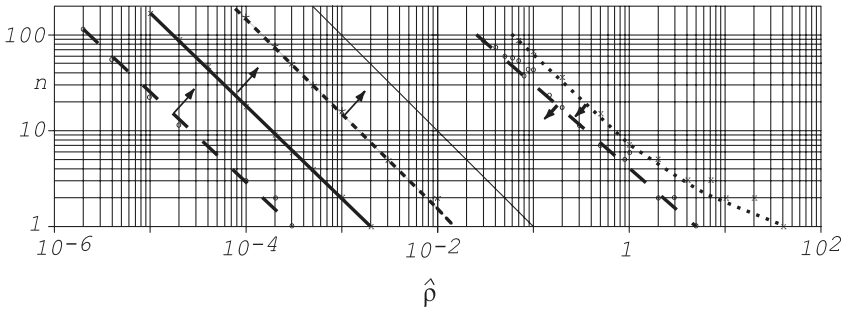

Fig. 8. Constant relative error, ε, in the n vs. $\hat{\rho}$ plane over eight orders of magnitude in $\hat{\rho}$. The three straight lines on the left show the results using Gaussian integration of Eq. (44). Dashed line: $\varepsilon = 10^{-6}$ with 64 points over the range $[0,7]$. Thick solid line: $\varepsilon = 10^{-9}$ using 64 points in $[0,7]$ and also closely represents $\varepsilon = 10^{-6}$ using 32 points in $[0,5]$. Dotted line: $\varepsilon = 10^{-9}$ using 32 points in $[0,5]$. The two lines on the right correspond to $\varepsilon = 10^{-9}$, for the trapezoidal (dotted line) and recursion (dashed line) methods. The arrows indicate the direction where the relative error decreases. The thin solid line corresponds to $n\hat{\rho} = 10^{-1}$.

A comparison of the relative error contours in Figs. 7 and 8 show that the accuracy of the these methods changes rapidly with $n\hat{\rho}$. A further comparison of the error contours in Fig. 8 enables us to obtain the prescription for perhaps the most accurate calculation of $\mathscr{G}^n$ over the whole range of n and ρ; since there is considerable overlap between these methods, one could use the recursion or trapezoidal method for, say,

Table 7
Relative errors for the trapezoidal, recursion and Gaussian (32 pts) methods for various values of n and $\hat{\rho}$ keeping $n\hat{\rho} = 0.1$

n	$\hat{\rho}$	Trapezoidal, m	Recursion	Gaussian
1	1.00E−01	$\sim 10^{-15}$, 64	−2.4E−15	−7.2E−13
2	5.00E−02	$\sim 10^{-16}$, 128	−1.8E−15	−7.0E−13
10	1.00E−02	$\sim 10^{-15}$, 256	−3.2E−15	−6.9E−13
20	5.00E−03	$\sim 10^{-15}$, 512	−4.2E−14	−6.9E−13
100	1.00E−03	$\sim 10^{-14}$, 512	8.2E−13	−6.8E−13

The number of grid points, m, for the trapezoidal method to achieve the indicated accuracy is also shown.

$n\hat{\rho} < 10^{-1}$ and the 32 points Gaussian method for $n\hat{\rho} \geqslant 10^{-1}$. This will easily ensure a relative error of better than 10^{-12} for all $n\hat{\rho}$ in the practical ranges of interest. Indeed, as shown in Table 7, the relative error with $1 < n < 100$ along the line where $n\hat{\rho} = 10^{-1}$ is $<10^{-13}$ for the trapezoidal method, $<10^{-12}$ for the recursion method, and $<10^{-12}$ for the Gaussian integration of Eq. (44). This boundary, $n\hat{\rho} = 10^{-1}$, is shown in Fig. 8 as the thin solid line.

The Greens function $\mathscr{G}^n(\hat{\rho})$ is directly related to the associated Legendre functions of the first kind, $P^n_{-1/2}(s)$. We have shown this relationship by the equivalence between the natural variable $\hat{\rho}$ of our cylindrical geometrical space and the natural variable, s, rooted in spherical coordinates. This enabled the new integral representation that was derived for $\mathscr{G}^n(\hat{\rho})$ to be carried over to $P^n_{-1/2}(s)$, and then generalized for $P^n_\nu(s)$. This relationship enabled use of well known properties of the Legendre functions to be directly applicable to $\mathscr{G}^n(\hat{\rho})$.

Acknowledgements

This work was supported by US DoE Contract No. DE-AC02-76-CH03073, and US DoE Grant Nos. DE-FG03-95ER54309 and DE-FG03-94ER54271.

Appendix A. Relationship to the associated Legendre functions

In order to make this work relevant to a broader context the connection of the Green's function to the associated Legendre functions is shown in this Appendix A. Expressing $\mathscr{G}^n$ in terms of the associated Legendre function of the first kind enabled the use of some of well known relations in the application of the Green's function used in the VACUUM code [5]. The two dimensional Green's function in (X–Z) space is given by

$$\mathscr{G}^n \equiv \frac{1}{2\pi} \oint \frac{1}{|\mathbf{r} - \mathbf{r}'|} e^{in(\phi - \phi')} d\phi', \tag{A.1}$$

where

$$|\mathbf{r} - \mathbf{r}'|^2 = X^2 + X'^2 + (Z - Z')^2 - 2XX' \cos(\phi - \phi'). \tag{A.2}$$

An integral representation of the associated Legendre function as a function of its conventional variable s, which has its origins in spherical coordinates, is given by [15,16]

$$P^n_\nu(s) = \frac{\Gamma(\nu + n + 1)}{2\pi\Gamma(\nu + 1)} \oint [s + \sqrt{s^2 - 1}\cos\phi]^\nu e^{in\phi} \, d\phi. \tag{A.3}$$

To express $\mathscr{G}^n$ in terms of this with $\nu = -1/2$, we set

$$X^2 + X'^2 + (Z - Z')^2 - 2XX' \cos\phi = f[s + \sqrt{s^2 - 1}\cos\phi] \tag{A.4}$$

to solve for s and f and find that

$$s = \frac{2\hat{\rho}^2 + 1}{2\sqrt{\hat{\rho}^2(\hat{\rho}^2 + 1)}} = \frac{2\hat{\rho}^2 + 1}{2\hat{\mathscr{R}}^2} = B, \tag{A.5}$$

$$\text{and} \quad f = 4XX'\hat{\rho}\sqrt{\hat{\rho}^2 + 1}, \tag{A.6}$$

$$\text{with} \quad \mathscr{R}^2 = 4XX'\sqrt{\hat{\rho}^2(\hat{\rho}^2 + 1)} \equiv 4XX'\hat{\mathscr{R}}^2. \tag{A.7}$$

Using these relations, Eq. (A.1) becomes

$$\mathscr{G}^n = \frac{\Gamma(1/2 - n)}{\pi^{1/2}\mathscr{R}} P^n_{-1/2}(s), \tag{A.8}$$

where the reflection formula for the gamma function, $\Gamma(z)\Gamma(1 - z) = -z\Gamma(-z)\Gamma(z) = \pi\csc(\pi z)$ was used. A few other relations that occur between the variables $\hat{\rho}$ and s are,

$$2\hat{\rho}^2 + 1 = \frac{s}{\sqrt{s^2-1}}, \tag{A.9}$$

$$\hat{\rho}^2(\hat{\rho}^2+1) = \hat{\mathscr{R}}^4 = \frac{1}{4(s^2-1)}, \tag{A.10}$$

$$\hat{\rho} \pm \sqrt{\hat{\rho}^2+1} = \left(\frac{s \pm 1}{s \mp 1}\right)^{1/4}. \tag{A.11}$$

From the relations above, it is seen that $0 < \hat{\rho} < \infty$ maps onto $\infty > s > 1$.

The Legendre functions for values of $n > 1$ can be generated from the upward recurrence relation,

$$P^{n+1}_{-1/2}(s) = -\frac{2ns}{(s^2-1)^{1/2}} P^n_{-1/2}(s) - (n-1/2)^2 P^{n-1}_{-1/2}(s), \tag{A.12}$$

or using Eqs. (A.8) and (A.9),

$$\mathscr{G}^{n+1} = \frac{4n(2\hat{\rho}^2+1)}{(2n+1)}\mathscr{G}^n - \frac{2n-1}{2n+1}\mathscr{G}^{n-1}, \tag{A.13}$$

for $n = 1, 2, \ldots$ and,

$$P^1_{-1/2}(s) = \frac{1/2}{(s^2-1)^{1/2}}\left\{P^0_{1/2}(s) - sP^0_{-1/2}(s)\right\}, \tag{A.14}$$

for $n = 0$. These are initiated by their relations to the complete elliptic integrals of the first and second kinds, K and E, respectively,

$$P^0_{-1/2}(s) = \frac{2}{\pi} m_1^{1/4} K(k), \tag{A.15}$$

$$P^0_{1/2}(s) = \frac{2}{\pi} m_1^{-1/4} E(k), \tag{A.16}$$

where

$$k^2 = \frac{1}{\hat{\rho}^2+1}, \quad \text{and} \quad m_1 = 1 - k^2. \tag{A.17}$$

Some of the relations used here can be derived from equations found in Erdélyi [16] and Abramowitz and Stegun [8]. The latter reference also contains polynomial approximations for the elliptic integrals which are accurate to $O(10^{-8})$; for near machine precision the iterative algorithms of Bulirsch [10] can be used instead.

The integral representation, Eq. (44) can also be expressed as a Legendre function. Using the relations in Eq. (33) and in Eqs. (A.5)–(A.11) $P^n_{-1/2}(s)$ can be written as,

$$P^n_{-1/2}(s) = \frac{2}{\sqrt{\pi} n \Gamma(1/2-n)}\left(\frac{s-1}{s+1}\right)^{n/2} \int_0^\infty \frac{t e^{-t^2}\,dt}{\sqrt{2s\sinh^2(t^2/2n) + \sinh(t^2/n)}}, \tag{A.18}$$

or,

$$P^n_{-1/2}(s) = \frac{1}{\sqrt{\pi}\Gamma(1/2-n)}\left(\frac{s-1}{s+1}\right)^{n/2} \int_0^\infty \frac{e^{-nt}\,dt}{\sqrt{2s\sinh^2(t/2) + \sinh t}}. \tag{A.19}$$

This last relation can be derived directly from the integral representation of Eq. (A.3) using a procedure similar to the one described in Section 6, the essential difference being that the relevant branch points within the range of integration, $0 < u < 2\pi$, occur instead at $u = \pi, v_0 = \pm s/\sqrt{s^2-1}$. Indeed, using this on Eq. (A.3) for arbitrary v (but $v > -1$) and taking the discontinuity across the branch cut properly into account, one can show that

$$P^n_v(s) = (-1)^{n+1}\frac{\Gamma(v+n+1)}{\pi\Gamma(v+1)}\left(\frac{s-1}{s+1}\right)^{n/2} \sin(\pi v) \int_0^\infty [2s\sinh^2(t/2) + \sinh t]^v e^{-nt}\,dt. \tag{A.20}$$

Using the reflection formula for the gamma function, this simplifies to,

$$P_\nu^n(s) = \frac{1}{\Gamma(\nu+1)\Gamma(-\nu-n)}\left(\frac{s-1}{s+1}\right)^{n/2}\int_0^\infty [2s\sinh^2(t/2)+\sinh t]^\nu e^{-nt}\,dt. \tag{A.21}$$

This constitutes a new integral representation of the associated Legendre function of the first kind and properly reduces to that found in Eq. (A.19) when $\nu = -1/2$.

References

[1] F. Troyon, L.C. Bernard, R. Gruber, Comput. Phys. Commun. 19 (1980) 161.
[2] R. Gruber, F. Troyon, D. Berger, L.C. Bernard, S. Rousset, R. Schreiber, W. Kerner, W. Schneider, K.V. Roberts, Comput. Phys. Commun. 21 (1981) 323.
[3] R. Gruber, S. Semenzato, F. Troyon, T. Tsunematsu, W. Kerner, P. Merkel, W. Schneider, Comput. Phys. Commun. 24 (1981) 363.
[4] R.C. Grimm, J.M. Greene, J.L. Johnson, Computation of the magnetohydrodynamic spectrum in axisymmetric toroidal confinement systems, in: J. Killeen (Ed.), Methods in Computational Physics, Controlled Fusion, vol. 16, Academic Press, New York, 1976, pp. 253–280.
[5] M.S. Chance, Phys. Plasmas 4 (1997) 2161.
[6] H.R. Wilson, P.B. Snyder, R.L. Miller, G.T.A. Huysmans, Phys. Plasmas (2002) 1277.
[7] P.B. Snyder, H.R. Wilson, et al., Phys. Plasmas (2002) 2037.
[8] M. Abramovitz, I.A. Stegun, Handbook of Mathematical Functions, ninth ed., Number 55 in Applied Mathematics Series, National Bureau of Standards, Superintendent of Documents, U.S. Government Printing Office, Washington, D.C. 20402, 1970.
[9] W.H. Press, B.P. Flannery, S.A. Teukolsky, W.T. Vetterling, Numerical Recipes: The Art of Scientific Computing, Cambridge University Press, 1988.
[10] R. Bulirsch, Numer. Math. 7 (1965) 78.
[11] G. Dahlquist, Å. Björck, Numerical Methods, 1st ed., Prentice-Hall Inc., Englewood Cliffs, New Jersey, 1974, pp. 297–301 (chapter 7).
[12] B.C. Carlson, SIAM J. Math. Anal. 9 (1978) 525.
[13] W.H. Press, S.A. Teukolsky, W.T. Vetterling, B.P. Flannery, Numerical Recipes in Fortran 77: The Art of Scientific and Parallel Computing, Cambridge University Press, 1996.
[14] H.B. Dwight, Tables of Integrals and Other Mathematical Data, 4th ed., The Macmillan Company, New York, 1966.
[15] E.T. Whittaker, G.N. Watson, A Course of Modern Analysis, 4th ed., Cambridge University Press, England, 1963.
[16] A. Erdélyi, Higher Transcendental FunctionsThe Bateman Manuscript Project, vol. 1, McGraw-Hill Book Co. Inc., New York, Toronto, Canada, London, England, 1953 (chapter 3).